Mineralium Deposita (2024) 59:329–340
https://doi.org/10.1007/s00126-023-01210-x

ARTICLE

Lithium-rich claystone in Pingguo area, Guangxi, southwest China: precursor kaolinite controls lithium enrichment

Kunyue Ling[1] · Hanjie Wen[2,3] · Tao Han[1] · Zhitong Lu[1] · Yi Cui[4] · Chongguang Luo[1] · Wenbin Yu[1]

Received: 11 October 2022 / Accepted: 25 August 2023 / Published online: 21 September 2023

Abstract

We investigated Late Permian Li-rich claystones with up to 1.05 wt% Li_2O (average: 0.45 wt% Li_2O) in the Pingguo area in Guangxi, southwest China. Our results show that cookeite (chlorite group) is the dominant Li-bearing mineral. Cookeite is intercalated with authigenic illite and detrital kaolinite, which suggests that cookeite formed during burial diagenesis from pre-existing Li-rich kaolinite in the original clay assemblage. The Li-rich claystones were mainly sourced from felsic volcanic rocks of the Emeishan large igneous province (LIP), and the Li-rich kaolinite was likely produced by weathering of felsic volcanic materials (i.e., pyroclastic rocks, tephras, and volcanic glass) deposited on a Permian carbonate platform. We propose that the abundance of precursor kaolinite and its Li content control the degree of Li enrichment in this new potential Li resource.

Keywords Lithium-rich claystone · Cookeite · Clay transformation · Li resource

Introduction

The consumption of Li is growing exponentially owing to increasing demand for Li-ion batteries in electric vehicles, laptops, and smartphones. Current demand and annual mine production are about 130,000 t Li (USGS 2023), which is expected to triple until 2030 (International Energy Agency 2022). At present, Li is mainly recovered from Li-rich pegmatites (e.g., lepidolite and spodumene) and Li-rich brines in both underground and surficial environments (Fig. 1; Kesler et al. 2012; Bowell et al. 2020). A third type consists of Li clay deposits in which Li is mainly structurally bound in clays such as hectorite [$Na_{0.3}(Mg,Li)_3Si_4O_{10}(OH)_2$] and jadarite [$LiNaB_3SiO_7(OH)$] owing to alteration of Li-rich silicic volcanic rocks and pyroclastic deposits by meteoric and hydrothermal fluids (Bowell et al. 2020; Castor and Henry 2020). In Li clay deposits, the mineral assemblage consists mainly of K-feldspar, quartz, calcite, albite, illite, hectorite, and/or jadarite (Table 1).

Bauxite-related Li-rich claystone is a new potential Li clay resource and has been discovered in wide parts of China, including in the lower Carboniferous Jiujialu Formation in central Guizhou Province, the upper Carboniferous Benxi Formation in Henan and Shanxi provinces, the lower Permian Dazhuyuan Formation in northern Guizhou Province, the lower Permian Daoshitou Formation in central Yunnan Province, and the upper Permian Heshan Formation in the western Guangxi Zhuang Autonomous Region (e.g., Wang et al. 2013; Cui et al. 2018; Yang et al. 2019; Wen et al. 2020; Zhang et al. 2022). These claystones have Li_2O contents of up to 2 wt% (Fig. 1; Table 1). As such, bauxite-related Li-rich claystones are a new key target for Li exploration (Table 1; Wen et al. 2020). For example, exploration in the Xiaoshiqiao and Guanyinshan area (7.2 km^2) in central Yunnan Province has identified 0.34 Mt of Li (average = 0.3% Li_2O) in this type of resource (Wen et al. 2020).

Editorial handling: R. Hu

✉ Hanjie Wen
wenhanjie@vip.gyig.ac.cn

1 State Key Laboratory of Ore Deposit Geochemistry, Institute of Geochemistry, Chinese Academy of Sciences, Guiyang 550081, China

2 School of Earth Science and Resources, Chang'an University, Xi'an 710054, China

3 College of Earth and Planetary Sciences, University of Chinese Academy of Sciences, Beijing 100049, China

4 State Key Laboratory of Nuclear Resources and Environment, East China University of Technology, Nanchang 330013, China

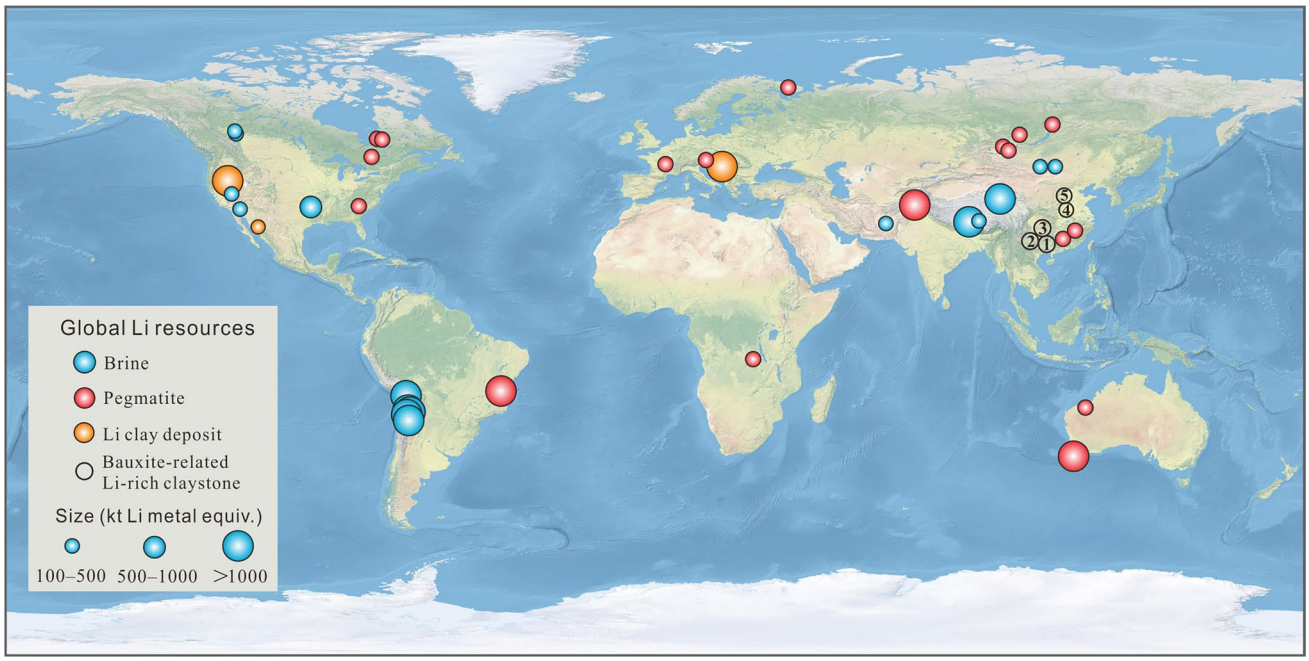

Fig. 1 Location map of global lithium resources (Benson et al. 2017) and bauxite-related Li-rich claystones (Song et al. 1987; Chen and Cai 1997; Wang et al. 2013; Cui et al. 2018; Yang et al. 2019; Wen et al. 2020; Ling et al. 2021; Cui et al. 2022). Bauxite-related Li-rich claystones were discovered in Guangxi (1), Yunnan (2), Guizhou (3), Henan (4), and Shanxi (5) provinces in China. The global map is modified after the World ocean bathymetric map by worldinmaps.com

The bauxite-related Li-rich claystones are generally associated with karst bauxite deposits (i.e., residual Al-rich sedimentary rocks unconformably deposited on carbonate rocks) and were formed by intense weathering of their source rocks (e.g., Wen et al. 2020; Ling et al. 2021). The bauxite-related Li-rich claystones consist mainly of clay (kaolinite, illite, and chlorite) and Al-rich minerals (diaspore and boehmite), along with accessory minerals (e.g., zircon and anatase; Table 1). The bauxite-related Li-rich claystones have geological features (e.g., mineral assemblages, Li contents, and fluid sources) that are distinct from those of Li clay deposits (Table 1; Song et al. 1987; Wen et al. 2020; Ling et al. 2021).

In the bauxite-related Li-rich claystones, Li is hosted by clay minerals as deduced from the positive correlation between whole-rock Li and clay mineral content (e.g., Wang et al. 2013; Wen et al. 2020; Ling et al. 2021; Zhang et al. 2022). However, the types of clay minerals that control the Li budget remain unclear. Based on the positive correlation between whole-rock Li and Mg content, it has been proposed that smectite is the main Li-bearing mineral in the bauxite-related Li-rich claystones (Cui et al. 2018; Wen et al. 2020). However, little or no smectite has been identified in the Li-rich claystones. Cookeite ($Al_2[(Si_3Al)O_{10}](OH)_2 \cdot (Al_2Li)(OH)_6$) is an uncommon Li-bearing chlorite, and it has been speculated that it is the carrier of Li in some Li-rich claystones, based on preliminary X-ray diffraction (XRD) analyses and its unique Al:Si ratio of 5:3 (Song et al. 1987; Ling et al. 2021; Cui et al. 2022). However, direct evidence to test these hypotheses is lacking, leading to uncertainty over the Li occurrence and its formation mechanisms. In this study, we investigated Li-rich claystones from the Pingguo area, Guangxi region, China, using in situ micro-analytical techniques, in order to identify the Li-bearing clay minerals and their origins.

Geological background

The Pingguo area in western Guangxi is located in the southwestern part of the South China Block, adjacent to the Song Ma suture zone in the south and the Permian Emeishan large igneous province (LIP; 263–251 Ma) in the northwest (Fig. 2A; Shellnutt 2014). At the end of the middle Permian, the Dongwu Orogeny caused domal uplift in the upper Yangtze area, which led to a large-scale marine regression in South China (Sun et al. 2010). The uplift in the central area was ~ 1 km, whereas it was > 100 m in western Guangxi region. This uplift led to the weathering and denudation of the middle Permian limestones of the Maokou Formation and the formation of paleo-karst (He et al. 2010). At the same time, the Emeishan LIP erupted over an area of > 250,000 km^2. The erupted magmas were mainly basaltic lavas and pyroclastic units, with felsic volcanic rocks,

Table 1 Information of global Li clay deposits and bauxite-related Li-rich claystones in China

Volcanic clay deposit	Li resource and grade	Mineral assemblage	Carrier of Li	Genesis
Sonora deposit[1] (Sonora, Mexico)	845 kt (0.49 wt% Li_2O)	K-feldspar, quartz, biotite, calcite, illite, smectite (hectorite)	Hectorite	Hydrothermal alteration of volcanic–sedimentary sequences
Jadar deposit[2] (Jadar, Serbia)	854 kt (1.76 wt% Li_2O and 16.1 wt% B_2O_3)	Calcite, dolomite, K-feldspar, Jadarite, rutile, albite, ilmenite, pyrite, muscovite	Jadarite	Hydrothermal alteration of volcanic–sedimentary sequences
Kings Valley/McDermitt deposit (Nevada, USA)[3,4,5]	100 kt (0.86 wt% Li_2O)	Calcite, albite, K-feldspar, quartz, illite, hectorite, tainiolite, Dolomite, fluorite	Hectorite, tainiolite	Hydrothermal alteration of volcanic–sedimentary sequences
Location of bauxite-related Li-rich claystone	Average grade of Li_2O (wt%)	Mineral assemblage	Carrier of Li	Genesis
Songqi, Henan, China[6]		Diaspore, boehmite, kaolinite, illite		
Zunyi, Guizhou, China[7]	0.43	Kaolinite, illite, chlorite, diaspore, boehmite,		
Baofeng, Henan, China[8]		Kaolinite, illite, diaspore, boehmite, chlorite		
Jinsha, Guizhou, China[9]	0.42	Kaolinite, illite, smectite, diaspore	Smectite?	
Saping, Guizhou, China[9]		Kaolinite, illite, smectite, diaspore	Smectite?	
Yuxi, Yunnan, China[10,11]	0.3	Kaolinite, illite, cookeite, smectite, diaspore	Cookeite, Smectite?	Burial diagenesis
Pingguo, Guangxi, China[12] (this study)	0.45	Kaolinite, illite, cookeite, diaspore, pyrohyrollite	Cookeite?	Burial diagenesis
Pinglu, Shanxi, China[13]	1.65	Kaolinite, illite, chlorite, diaspore		
Somewhere in Henan, China[14,15]		Illite, kaolinite, cookeite, pyrohyrollite, diaspore, dickite	Cookeite?	Burial diagenesis

References: [1]Verley and Geo 2014; [2]Rio Tinto 2022; [3]Benson et al. 2017; [4]Bowell et al. 2020; [5]Castor and Henry 2020; [6]Wang et al. 2012; [7]Huang et al. 2014; [8]Yang et al. 2019; [9]Cui et al. 2018; [10]Wen et al. 2020; [11]Cui et al. 2022; [12]Ling et al. 2021; [13]Chen and Chai 1997; [14]Shen et al. 1986; [15]Song et al. 1987

such as trachyte and rhyolite, being erupted in the late stages (Shellnutt 2014). The greenhouse climate and acid rain caused by the Emeishan LIP may have increased continental weathering and formed an Al-rich weathering profile, which was then eroded, transported, and deposited in the Youjiang Basin (Liu et al. 2017; Yu et al. 2019). The Emeishan LIP volcanic rocks in the western Guangxi area are relatively thin (300–500 m) and have been completely eroded. They provided a source for bauxite and overlying Li-rich claystones at the bottom of the Heshan Formation. The Heshan Formation unconformably overlies the limestones of the Maokou Formation (Yu et al. 2019).

The basal part of the Heshan Formation in the Pingguo area consists of clastic rocks that are subdivided into a lower layer (~ 8 m thick) of purple, grey, or black bauxite ores and an overlying claystone layer (~ 10 m thick) of black carbonaceous (Li-rich) claystones (Fig. 2B, C; Ling et al. 2021). The Li-rich claystone in the Pingguo area crops out in the Taiping, Jiucheng, and Haicheng areas (~ 100 km^2) and is typically 2–3 m thick and has Li_2O contents of 0.06–1.05 wt% (average = 0.45 wt%; Ling et al. 2021; Fig. 2B).

Materials and methods

Lithium-rich claystones from Xinxu and Jiaomei villages in Pingguo County, Guangxi region, southwest China, were collected in this study (Fig. 2B; Ling et al. 2021). Representative samples XX-15 (Li_2O = 0.43 wt%) and JM-11 (Li_2O = 1.05 wt%) were made into polished thin-sections for scanning electron microscopy (SEM) using a FEI Scios dual-beam SEM instrument equipped with an energy dispersive spectrometer (EDS) at the Institute of Geochemistry, Chinese Academy of Sciences, Guiyang, China. The foils (length = 15 μm for XX-15 and 3 μm for JM-11; width = 7 μm; thickness = 0.06 μm) used for the transmission electron microscopy (TEM) and time-of-flight secondary ion mass spectrometry (TOF–SIMS) analyses were

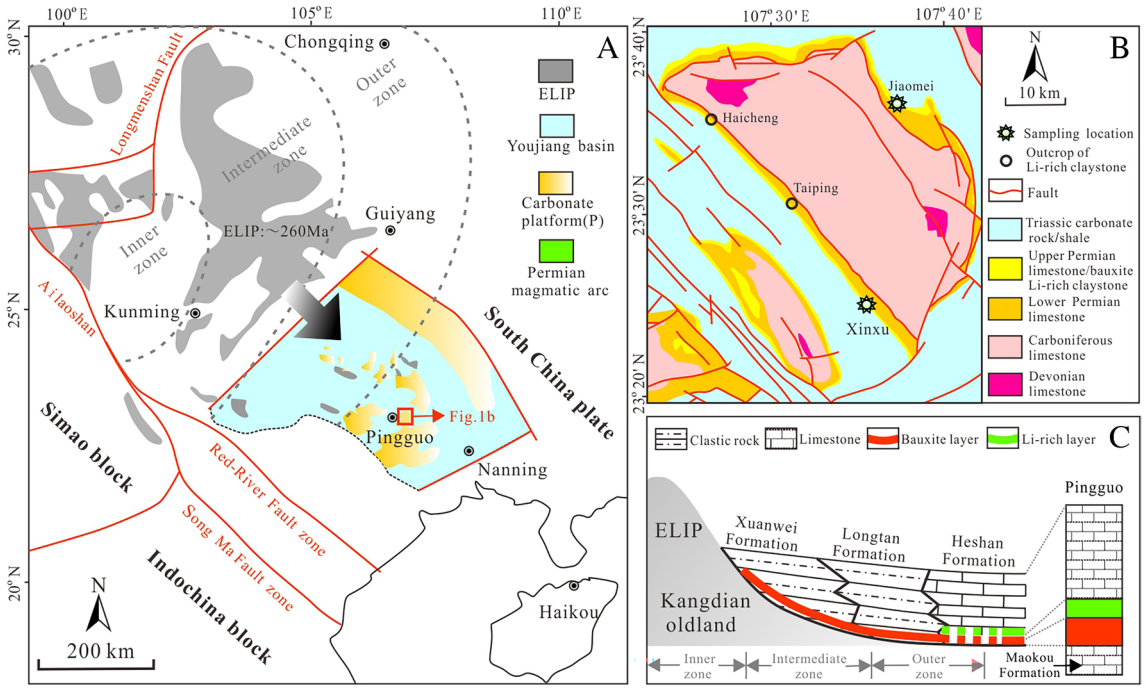

Fig. 2 **A** Map of the generalized tectonic domains in the southwestern Yangtze Plate and middle–late Permian paleogeography of the Youjiang Basin (modified after Ling et al. 2021). **B** Geological features of the Pingguo region, Guangxi. **C** Palaeogeographic map after the main phase of Emeishan LIP activity, showing the location of the Li-rich claystones in the Heshan Formation in the Pingguo area, Guangxi, China (modified after He et al. 2003 and Ling et al. 2021)

prepared using the focused ion beam (FIB) technique and SEM imaging. The foils were cut from the target area by the FIB, removed from the excavation site, and mounted on a Cu grid. The TEM analysis employed an FEI Talos F200S TEM instrument at the Guangdong University of Technology, Guangzhou, China. High-resolution TEM images were obtained and diffraction patterns imaged by selected area electron diffraction (SAED) analysis. The TOF–SIMS analysis was undertaken using an ION-TOF GmbH TOF–SIMS 5–100 instrument at the National Center for Electron Spectroscopy, Tsinghua University, Beijing, China.

Results

The SEM–EDS analyses showed that there are large differences in the mineral assemblages between samples XX-15 and JM-11 (Figs. 3, 4, 5, and 6). Sample XX-15 consists mainly of kaolinite, cookeite, and illite (Fig. 3), consistent with the XRD results (Fig. S1) of Ling et al. (2021). The sample has a typical clastic texture with coarse-grained (> 5 μm) minerals and a fine-grained matrix (< 2 μm). Both cookeite and illite are coarse-grained and lamellar in shape (5–20 μm). The matrix consists of fine-grained scaly-shaped kaolinite (< 1 μm; Fig. 3B, C, and E), which is euhedral–subhedral (Fig. 5B). In contrast, the coarse-grained cookeite and illite are usually anhedral with rounded or elliptical shapes (Fig. 3B–E).

Sample JM-11 consists mainly of cookeite, illite, diaspore, pyrophyllite, and kaolinite, along with smaller amounts of accessory zircon and anatase (Fig. 4), which is consistent with the XRD results (Table S1) of Ling et al. (2021). Similar to sample XX-15, this sample also has a clastic texture with coarse-grained minerals and matrix. The diaspore is lamellar or platy in shape and generally forms large nodular aggregates (usually > 100 μm; Fig. 4A, B, and G). The pyrophyllite usually is anhedral with rounded or elliptical morphology (usually > 10 μm; Fig. 4C). Cookeite, illite, and kaolinite can be both coarse-grained (5–20 μm) and fine-grained (i.e., in the matrix with a grain size of < 2 μm) (Fig. 4C–G). The anatase and zircon are typically small (< 5 μm), although some occur as automorphic or hypautomorphic granules (> 50 μm) (Fig. 4A, B).

Coarse-grained sites were selected for foil sampling with the FIB technique and SEM imaging, which were used for the TEM and TOF-SIMS analyses (Fig. 3D–F and 4G, H). For foil XX-15, high-angle annular dark field (HAADF) and SAED techniques identified the coarse particles as being chlorite (possibly cookeite) and a small amount of illite. These two types of minerals are parallel and intercalated with each other (Fig. 5). The illite with (001) interplanar spacing of ~ 10 Å (H01–04) is likely authigenic (i.e., the

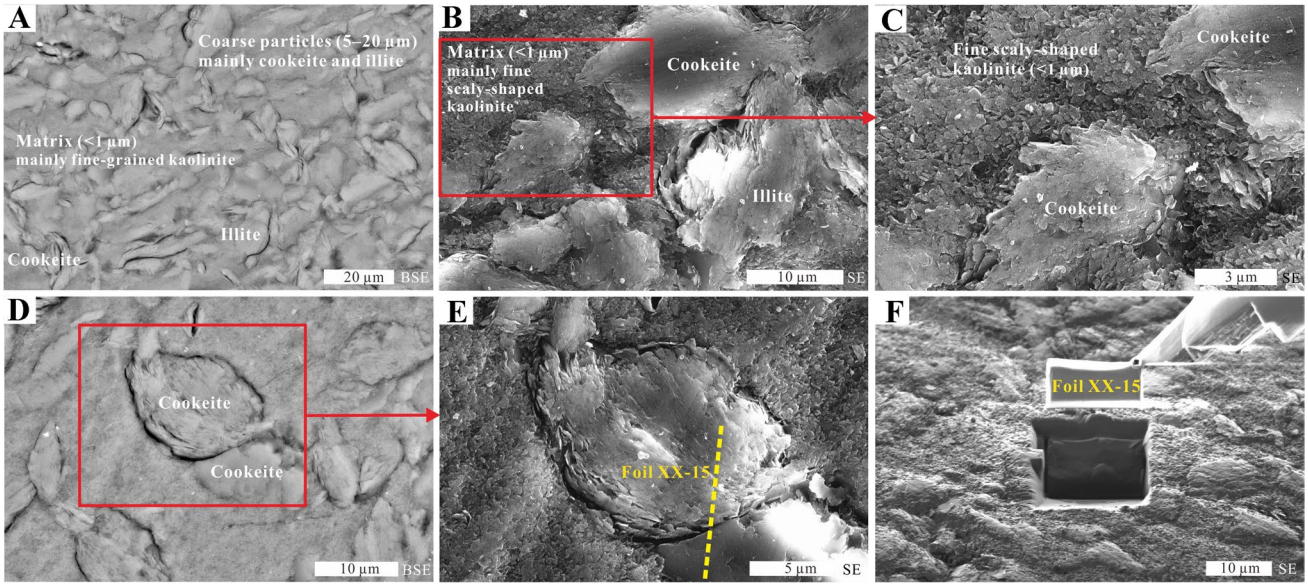

Fig. 3 Scanning-electron microcopy (SEM) images of a Li-rich claystone (sample XX-15) from the Pingguo area, Guangxi region, China. **A** Coarse-grained cookeite and illite set in a fine-grained matrix of kaolinite. **B** Coexisting coarse-grained, lamellar cookeite and illite. **C** Fine-grained, scale-like kaolinite matrix (i.e., detrital in origin) and coarse-grained, lamellar cookeite. **D** BSE image of the sampling site of foil XX-15. **E** SEM image of the sampling site of foil XX-15. **F** Sampling site of foil XX-15 after its removal. BSE, back-scattered electron image; SE, secondary electron image

1 M/1M_d variety) rather than detrital (i.e., the 2M_1 variety with a [001] interplanar spacing of ~ 20 Å) in origin (Fig. 3C–F; Tosca et al. 2010; Lu et al. 2021). Chlorite (cookeite) was identified based on its (002) interplanar spacing of ~ 14.2 Å (H02–04) (Fig. 5D–F). The matrix consists mainly of kaolinite with a (001) interplanar spacing of ~ 7 Å (H05) (Fig. 5G). TOF–SIMS analysis revealed that the Li-rich phase (i.e., coarse-grained chlorite) is characterized by high Al and Si contents, low Mg, Ca, and Na contents, and negligible Fe and K contents (Fig. 5H–O). In addition, the Li-rich phase has a lower Si content than the kaolinite matrix (Fig. 5I). This is consistent with the TEM–EDS analysis results that showed the atomic percentage of Si in the Li-rich phase (10.7–12.3 atomic %; average = 11.5 atomic %; areas #3–6) is lower than that of the kaolinite phase (14.1–14.4 atomic %; average = 14.3 atomic %; areas #7–9) (Fig. 5G; Table 2). In summary, several lines of evidence suggest that the Li-rich areas are the Li-bearing chlorite cookeite: (1) the Li-rich areas are mainly chlorite with a (002) interplanar spacing of ~ 14.2 Å; (2) the Li-rich areas exhibit extreme enrichment of Al, Si, and Li, moderate enrichment of Mg, Ca, and Na, and lack Fe and K; and (3) the Al/Si atomic ratios of the Li-rich areas vary from 1.6 to 1.7 (average = 1.64; Table 2), which is consistent with the value for cookeite (1.67).

Similar to foil XX-15, cookeite and 1 M/1M_d illite were also identified in foil JM-11 (Fig. 6I, J; H6–7). TEM–EDS analysis revealed that occasional Mg-rich chlorite (i.e., sudoite; $Al_2[(Si_3Al)O_{10}](OH)_2{\cdot}(Mg_2Al)(OH)_6$) was identified, based on its (002) interplanar spacing of 14.21 Å (H09), high Al (13.3–15.1 atomic %; areas #10–11) and Si (10.9–11.0 atomic %; areas #10–11) contents, atomic Al/Si ratios of 1.21–1.39 (theoretical ratio of 1.33), high Mg contents (6.77–7.11 atomic %; areas #10–11), and negligible Fe contents (Fig. 6G and L; Table 2). Area #12 comprises cookeite based on its (002) interplanar spacing of 14.14 Å (H07), high Al (17.2 atomic %) and Si (13.4 atomic %) contents, atomic Al/Si ratios of 1.28, low Mg content (0.66 atomic %), and negligible Fe content (Fig. 6; Table 2). In addition, area #16 comprises kaolinite owing to its (001) interplanar spacing of 7.18 Å (H08), lamellar grain shape, atomic Al/Si ratio of 0.99, and negligible contents of other elements apart from Al, Si, and O (Fig. 6; Table 2).

Discussion

Origin of the cookeite

Clay minerals in sediments/sedimentary rocks can be inherited/detrital (i.e., transported from the source to sink with little modification) or authigenic, i.e., formed in situ by neoformation (i.e., direct precipitation and crystallization from solution) or transformation (i.e., alteration of a precursor mineral structure without dissolution) (Bergaya and Lagaly 2013). In addition to pedogenic, sedimentary, and diagenetic

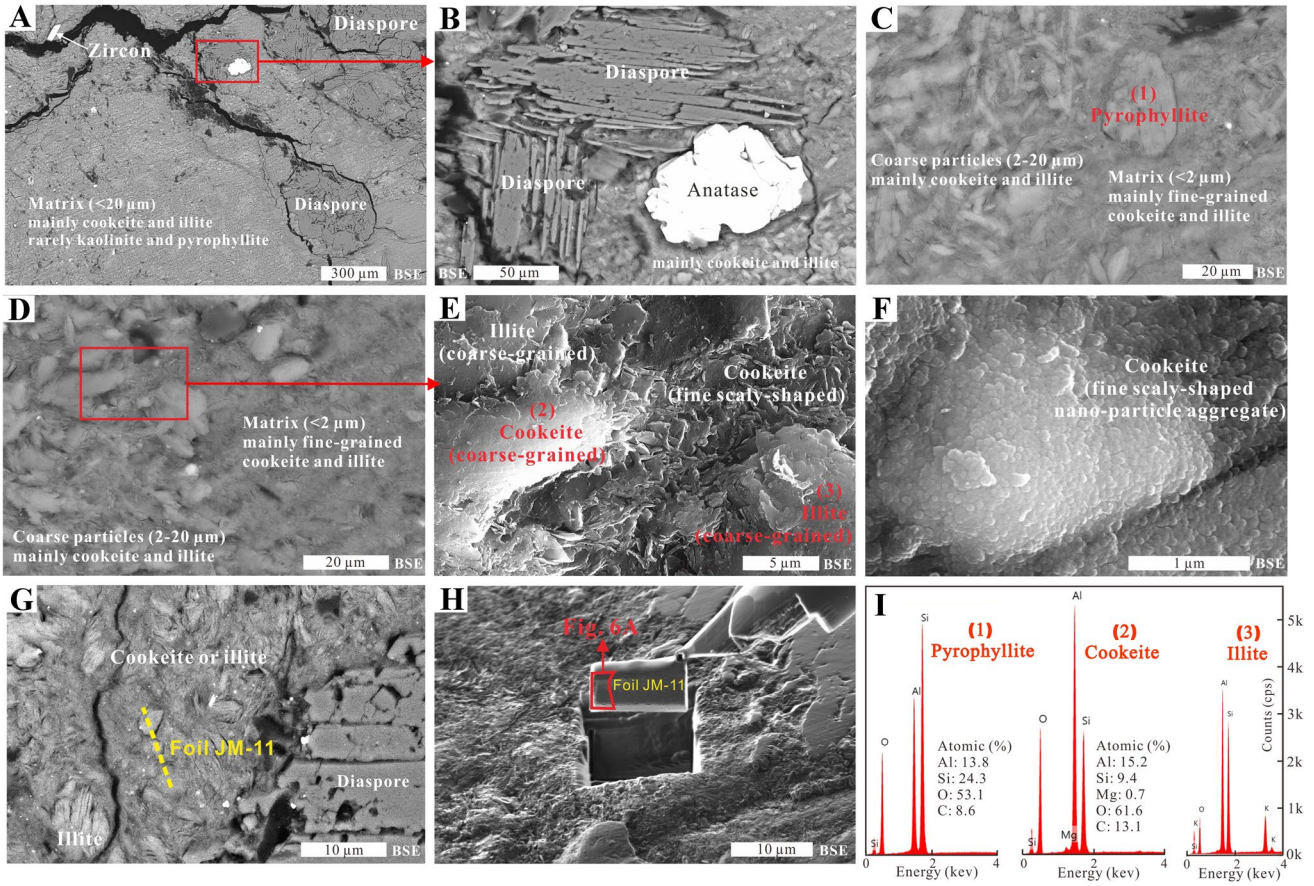

Fig. 4 Scanning-electron microcopy (SEM) images of a Li-rich claystone (sample JM-11) from the Pingguo area, Guangxi region, China. **A** Random distribution of diaspore aggregates, and detrital zircon and anatase in a matrix that consists mainly of clay minerals. **B** Coexisting anatase and diaspore (platy-shaped) aggregate. **C** Coexisting coarse-grained pyrophyllite and coarse- and fine-grained cookeite and illite. **D** Coarse particles set in a fine-grained matrix, both of which consist of cookeite and illite. **E** Coexisting coarse- and fine-grained cookeite and illite. **F** Fine-grained, scaly-shaped, nano-particle aggregates of cookeite that are indicative of an authigenic origin. **G** Sampling site of foil JM-11. **H** Sampling site of foil JM-11 after its removal. **I** EDS patterns of pyrophyllite, cookeite, and illite. BSE, back-scattered electron image; SE, secondary electron image

processes, hydrothermal alteration is another possible formation mechanism for chlorite. In this study, no evidence for mineral alteration was found in the Li-rich claystones, thus precluding chlorite formation by hydrothermal alteration (Figs. 3, 4, 5, and 6).

In sample XX-15, the fine-grained kaolinite in the matrix is euhedral–subhedral, which is indicative of an authigenic origin (i.e., neoformation or transformation; Figs. 3 and 5B). The sharp contacts between the fine- and coarse-grained minerals indicate that unlike the fine-grained kaolinite in the matrix, the coarse-grained cookeite and illite with an anhedral have a detrital or transformed origin (Fig. 3). In addition, the fine-grained kaolinite is commonly cross-cut by coarse-grained cookeite (intergrown with illite), further supporting this interpretation (Fig. 5B).

Kaolinite and Al-hydroxide minerals are usually formed by intense chemical weathering in warm and humid climates, whereas chlorite and illite can only be formed by physical erosion in cold and arid climates (Chamley 1989; Bergaya and Lagaly 2013). The presence of kaolinite and diaspore (i.e., an Al-hydroxide) and the extremely high values of chemical index of alteration (CIA = 92.8–98.1; Table S2; Ling et al. 2021) suggest that the Li-rich claystones were formed by intense chemical weathering in a warm and humid climate, which hindered the formation of chlorite and illite (Yang and Zhang 1994; Bergaya and Lagaly 2013; Wen et al. 2020; Ling et al. 2021). In fact, transformed chlorite and illite are typically the products of mineral transformation during burial diagenesis (Robinson et al. 2002; Worden et al. 2020). As such, the cookeite and illite in sample XX-15 were likely transformed from pre-existing materials rather than being of detrital origin.

In sample JM-11, the coarse-grained minerals (cookeite, illite, and pyrophyllite) typically have rounded or elliptical shapes, similar to the coarse-grained cookeite and illite in

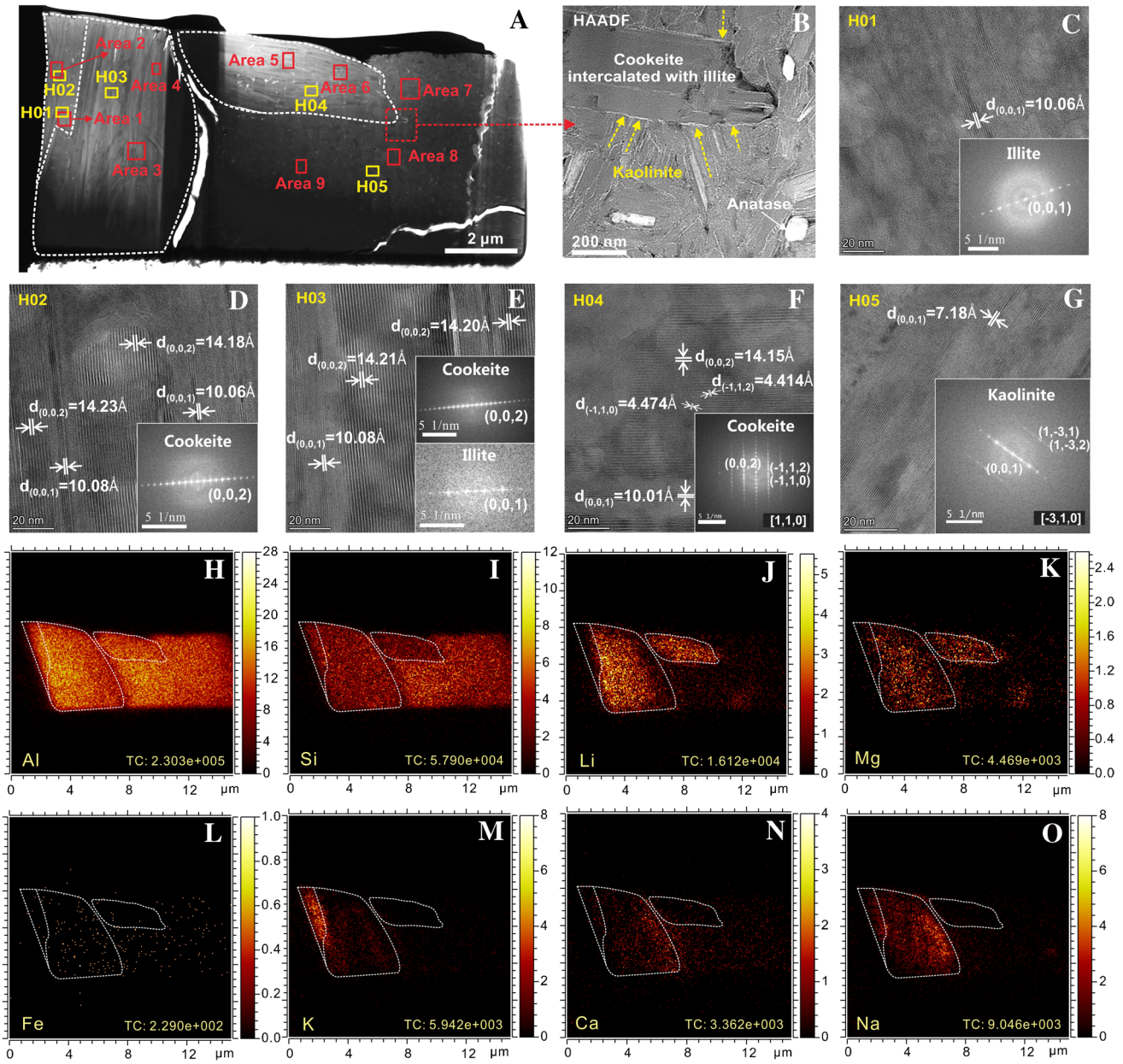

Fig. 5 Scanning-electron microcopy (SEM) image (**A**), high-angle annular dark-field imaging (HAADF) (**B**), high-resolution transmission-electron microscopy (TEM) images (**C**–**G**), and time-of-flight secondary-ion mass spectrometry (TOF–SIMS) images (**H**–**O**) of foil XX-15 showing the mineralogical and textural characteristics of sample XX-15 at the micro and nano scales

sample XX-15, thus also indicating a transformation origin. In high-resolution SEM images of sample JM-11, it is evident that the cookeite matrix consists of stacked nano-scale layers of scaly-shaped cookeite (Fig. 4F), which are suggestive of an authigenic origin (i.e., neoformation or transformation). In addition, the coarse- and fine-grained minerals do not have clear boundaries (Fig. 4E), thus indicating a similar transformation origin from pre-existing materials.

Kaolinite transformation to cookeite

In sample JM-11, the coarse-grained phase consists of cookeite (intercalated with illite), sudoite, and kaolinite which occur parallel to each other (Fig. 6A, B). This indicates that the cookeite, illite, and sudoite formed from pre-existing kaolinite during burial diagenesis. Furthermore, the coexisting cookeite, illite, and kaolinite have similar

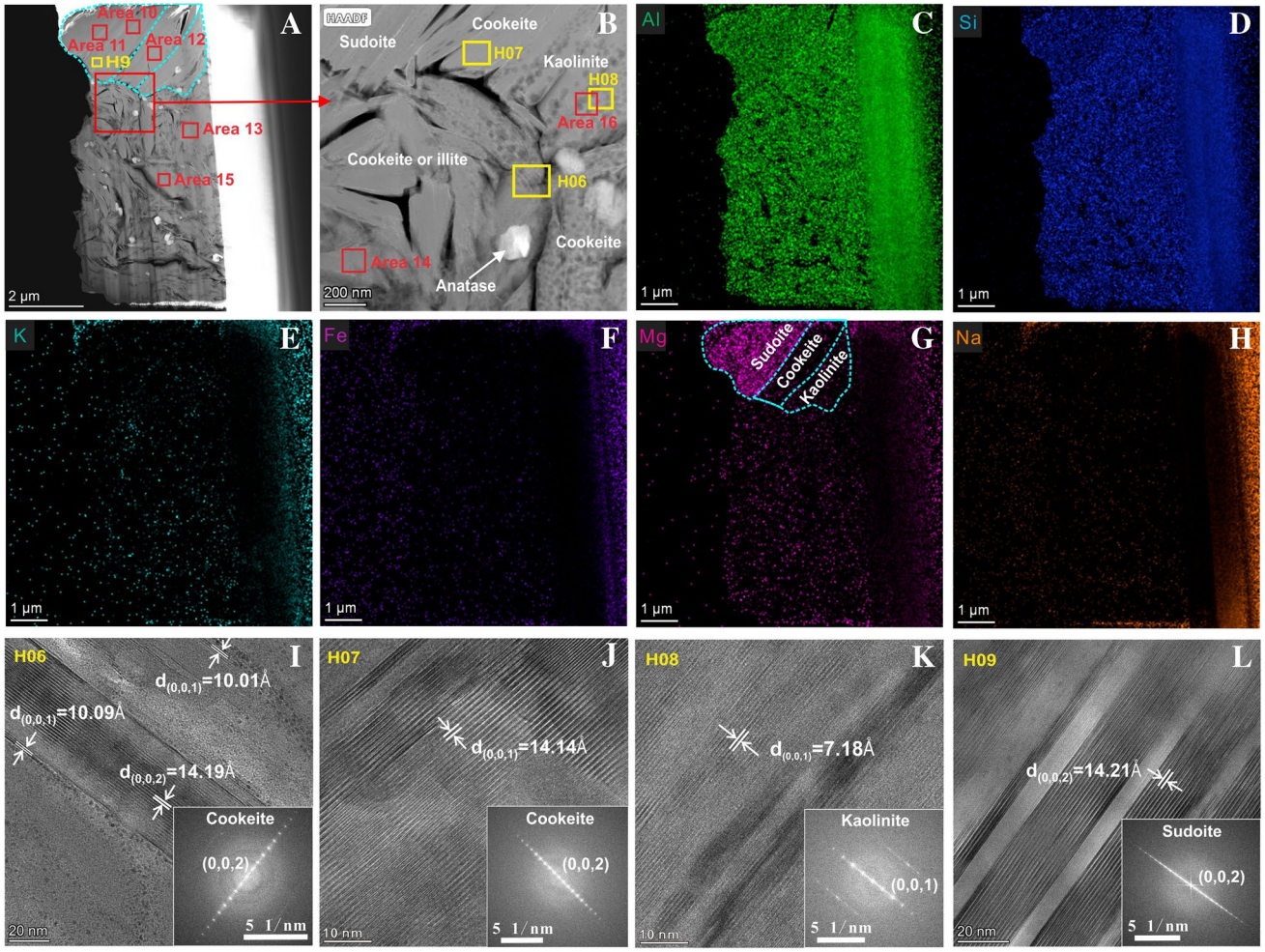

Fig. 6 High-angle annular dark-field (HAADF) images (**A**, **B**), transmission-electron microscopy with energy-dispersive spectrometry (TEM-EDS) images (**C**–**H**), and high-resolution TEM images (**I**–**L**) of foil JM-11 showing the mineralogical and textural characteristics of sample JM-11 at the micro and nano scales

Table 2 Results of transmission-electron microscopy with energy-dispersive spectrometry (TEM–EDS) analysis (atom %)

Area	Al	Si	Fe	K	Na	Ca	Mg	Ti	O	Al/Si ratio	Mineral species
Area #1	16.6	16.8	0.09	1.96	0.47	0.07	0.21	0.07	63.7	0.99	Illite
Area #2	17.3	15.8	0.04	1.74	0.44	0.05	0.23	0.05	64.4	1.1	Illite
Area #3	19.9	12.3	0.04	0.06	0.42	0.1	0.62	0.06	66.5	1.62	Cookeite
Area #4	19.4	12.1	0.08	0.04	0.75	0.08	0.5	0.09	66.9	1.6	Cookeite
Area #5	18.5	10.9		0.08					70.5	1.7	Cookeite
Area #6	17.4	10.7		0.05					71.9	1.62	Cookeite
Area #7	15.4	14.1		0.03					70.5	1.1	Kaolinite
Area #8	15	14.4		0.08					70.5	1.04	Kaolinite
Area #9	15.4	14.3		0.07					70.3	1.08	Kaolinite
Area #10	15.1	10.9		0.15			6.77		67.1	1.39	Sudoite
Area #11	13.3	11		0.07			7.11		68.5	1.21	Sudoite
Area #12	17.2	13.4		0.16			0.66		68.5	1.28	Cookeite
Area #13	18.8	12.9		0.06			0.27		68	1.46	Cookeite
Area #14	17.6	11.7		0.17			0.85	0.04	70.6	1.5	Cookeite
Area #15	15.7	15		0.17			0.28		68.9	1.04	Kaolinite
Area #16	15.2	15.3		0.14				0.08	69.3	0.99	Kaolinite

shapes in the matrix, thus further supporting this interpretation (Fig. 6A, B). Illitization of kaolinite is a common clay transformation during burial diagenesis and low-grade metamorphism (Dunoyer de Segonzac 1970; Sommer 1978; Dutta and Suttner 1986; Lanson et al. 1996, 2002). In addition, kaolinite transformed into chlorite has been observed in field studies of burial diagenesis and low-grade metamorphism (Muffler and White 1969; Curtis et al. 1985; Smith and Ehrenberg 1989). The basic transformation of kaolinite leads to the formation of dickite and pyrophyllite under diagenetic/low-grade metamorphic conditions (Bergaya and Lagaly 2013). As such, the presence of pyrophyllite indicates that the Li-rich claystones experienced diagenesis and low-grade metamorphism. Therefore, we propose that cookeite and illite were transformed from pre-existing detrital kaolinite during diagenesis. Hence, in sample XX-15, two types of kaolinite were present in the original clay assemblage: (1) coarse-grained detrital kaolinite and (2) fine-grained authigenic kaolinite.

Transformation from kaolinite to cookeite during burial diagenesis requires an additional Li input. In the present study, only transformation of detrital kaolinite (rather than authigenic kaolinite) to cookeite occurred. The most plausible explanation for this difference is that the detrital kaolinite was enriched in Li, which is essential for cookeite formation, whereas the authigenic kaolinite was not enriched in Li, as shown by the in situ analyses (Fig. 5J).

Origin of Li-rich kaolinite

Felsic volcanic material (i.e., rocks, tephras, and glasses) is typically rich in Li and could be an important source of Li in clay deposits (Aoudjit et al. 1995; Fesharaki et al. 2007). For example, in the McDermitt Li clay deposit in the USA, a large amount of Li was leached from rhyolitic volcanic rocks and tephras by meteoric and hydrothermal fluids and then bound in hectorite (i.e., a Li-bearing smectite) in tephra-rich sediments (Benson et al. 2017). Detrital zircon studies of the basal part of the Heshan Formation throughout western Guangxi Province (including the Pingguo area) have yielded consistent results with a single age peak (*ca.* 260 Ma) and a negative Hf isotopic composition, indicative of a felsic volcanic rock source from the Emeishan LIP (Deng et al. 2010; Hou et al. 2017; Ling et al. 2021). The weathering of felsic volcanic rocks in a warm and humid climate is conductive to the formation of kaolinite (Chamley 1989; Bergaya and Lagaly 2013; Li et al. 2020; Huang et al. 2021). We therefore propose that the Li-rich kaolinite was likely produced by weathering of felsic volcanic materials from the Emeishan LIP. Given the high cation exchange capacity of kaolinite, Li is predominantly adsorbed as an ion onto its surface (Ma and Eggleton 1999).

Transformation mechanism

The structures of clay minerals are based on the tetrahedral (Si–O layers; abbreviated as "T") and octahedral (Al–O,

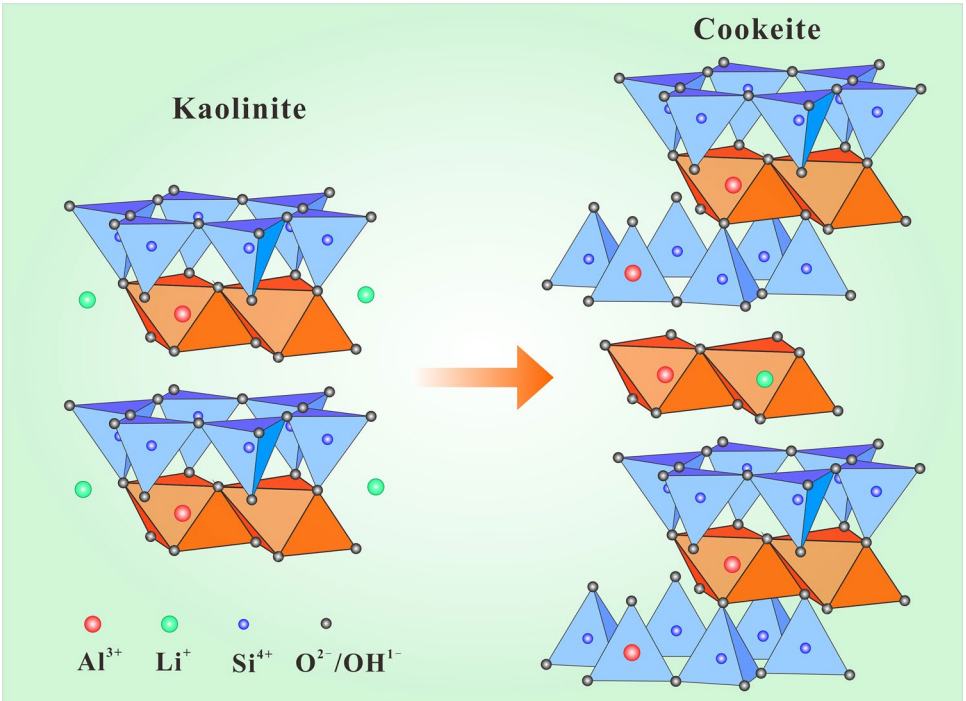

Fig. 7 A schematic diagram showing the mineral structures involved in the transformation of Li-rich kaolinite to cookeite during diagenesis of the Li-rich claystones from the Pingguo area, Guangxi, China

Fe–O, or Mg–O layers; abbreviated as "O") sheets that may be condensed into either 1:1 or 2:1 types to form an anisotropic TO or TOT layer (Bergaya and Lagaly 2013; He et al. 2014; Tao et al. 2022). The octahedral structure is referred to as either trioctahedral if all of the three octahedral sites are occupied or dioctahedral if only two of the three octahedral sites are occupied. Illite is a 2:1 dioctahedral clay mineral with a TOT structure. Cookeite is a $TOTO_{int}$ (O_{int} is an octahedral interlayer sheet of hydroxide) structured dioctahedral–trioctahedral chlorite, in which the 2:1 layer is dioctahedral and the hydroxide interlayer is trioctahedral (Bergaya and Lagaly 2013).

Two mechanisms have been proposed for clay transformations: (1) solid-state transformation by atomic rearrangement with the interlayer being the main route for atomic diffusion in and out of the clay structure and (2) dissolution-crystallization by dissolution of the original mineral and recrystallization of the new structural phase (Nadeau et al. 1985; Dudek et al. 2006; He et al. 2017; Ji et al. 2018). In this study, the cookeite is parallel and intercalated with kaolinite, suggesting solid-state transformation. The transformation of 1:1 type clay minerals to 2:1 type ones in solid state can occur under hydrothermal conditions with mildly alkaline pH and enrichment of Si, through the formation of a new tetrahedral sheet attached to the pre-existing 1:1 layer (He et al. 2017). Cookeite is a 2:1:1 clay mineral, characteristized by regularly stacked 2:1 layer and a single interlayer octahedral sheet (Fig. 7; Bergaya and Lagaly 2013). Hence, solid-state transformation of kaolinite (1:1 type) to cookeite involves the formation of a 2:1 layer and an octahedral hydroxide sheet (Al and Li occupy the octahedral sites), which requires additional Al and Li supply for its formation (Fig. 7). In addition, from the perspective of stoichiometry, the transformation from kaolinite ($Al_4[Si_4O_{10}](OH)_8$) to cookeite ($LiAl_4[Si_3AlO_{10}](OH)_8$) also involves an increase in Al and Li contents.

The occurrence of diaspore (Al-hydroxide) in the Li-rich claystones is suggestive of alkaline pH and Al-saturated diagenetic conditions (Table S1; Fig. 4A, B, and G), which is conducive to the formation of 2:1 layer and octahedral hydroxide sheet in clays (Bergaya and Lagaly 2013; He et al. 2017). Thus, the process of transforming Li-rich kaolinite into cookeite under alkaline pH and Al-saturated conditions during diagenesis can be described as follows (Fig. 7): (1) additional supply of Al and rearrangement of Li lead to the formation of octahedral hydroxide sheets intercalating into the interlayer space between two kaolinite layers and (2) simultaneously, Si-O tetrahedral sheets are formed and attached to the pre-existing 1:1 layer (additional Si can be produced by water-rock interactions), accompanied by the substitution of Al^{3+} for Si^{4+} in the newly formed tetrahedral sheets.

Implications and conclusions

This study has demonstrated that cookeite is the dominant Li-bearing mineral in the claystones in the upper Permian Heshan Formation in the Pingguo area, Guangxi, China. Cookeite is intercalated with authigenic illite and detrital kaolinite, which indicates that cookeite was likely transformed from pre-existing, detrital, Li-rich kaolinite in the original clay assemblage during burial diagenesis (including diagenetic and low-grade metamorphic processes). Given that the Li-rich claystones in the Pingguo area were sourced mainly from felsic volcanic materials of the Emeishan LIP, the Li-rich kaolinite was likely produced by weathering of felsic volcanic materials (i.e., pyroclastic rocks, tephras, and glass) from this LIP. We propose that the abundance of precursor kaolinite and its Li contents controlled the degree of Li enrichment in these claystones. This finding could help to target exploration of this potential Li resource.

Supplementary Information The online version contains supplementary material available at https://doi.org/10.1007/s00126-023-01210-x.

Acknowledgements The authors would like to thank Prof. Hongping He, Dr. Wenjun Hu, and Dr. Shanling Fu for their valuable advice.

Funding This work was supported by the National Natural Science Foundation of China (grants 92162214, 92062107, U1812402), the National Key R&D Program of China (2022YFC2903402), the Key R&D Program of Yunan Province (grant 202103AQ100003), and the Guizhou Provincial Science and Technology Project (ZK[2021] key program 046).

Declarations

Competing interests The authors declare no competing interests.

References

Aoudjit H, Robert M, Elsass F, Curmi P (1995) Detailed study of smectite genesis in granitic saprolites by analytical electron microscopy. Clay Miner 30:135–147

Benson TR, Coble MA, Rytuba JJ, Mahood GA (2017) Lithium enrichment in intracontinental rhyolite magmas leads to Li deposits in caldera basins. Nat Commun 8:270

Bergaya F, Lagaly G (2013) General introduction. Clays, clay minerals, and clay science. Elsevier, pp 1–813

Bowell RJ, Lagos L, Hoyos C, Declercq J (2020) Classification and characteristics of natural lithium resources. Elements 16:259–264

Castor SB, Henry CD (2020) Lithium-rich claystone in the McDermitt Caldera, Nevada, USA: geologic, mineralogical, and geochemical characteristics and possible origin. Minerals 10:68

Chamley H (1989) Clay formation through weathering. Clay Sedimentology. Berlin, Heidelberg, Springer

Chen P, Chai D (1997) Sedimentary geochemistry of carboniferous bauxite deposits in Shanxi massif. Shanxi Science and Technology Press (in Chinese), Taiyuan

Cui Y, Luo C, Xu L, Zhang H, Deng M, Gu H, Meng Y, Qin C, Wen H (2018) Weathering origin and enrichment of lithium in clay rocks of the Jiujialu Formation, Central Guizhou Province, Southwest China. Bull Miner Petrol Geochem 37:696–704 (in Chinese with English abstract)

Cui Y, Wen H, Yu W, Luo C, Du S, Ling K, Yang J, Jia Y, Zhao Y, Ma W (2022) Study on the occurrence and enrichment mechanism of lithium in the lithium-rich claystones of the Lower Permian Daoshitou Formation in Central Yunnan. Acta Petrol Sin 38(07):2080–2094 (in Chinese with English abstract)

Curtis CD, Hughes CR, Whiteman JA, Whittle CK (1985) Compositional variation within some sedimentary chlorites and some comments on their origin. Mineral Mag 49:375–386

Deng J, Wang Q, Yang S, Liu X, Zhang Q, Yang L, Yang Y (2010) Genetic relationship between the Emeishan plume and the bauxite deposits in Western Guangxi, China: constraints from U-Pb and Lu–Hf isotopes of the detrital zircons in bauxite ores. J Asian Earth Sci 37:412–424

Dudek T, Cuadros J, Fiore S (2006) Interstratified kaolinite-smectite: nature of the layers and mechanism of smectite kaolinization. Am Mineral 91:159–170

Dunoyer de Segonzac G (1970) The transformation of clay minerals during diagenesis and low-grade metamorphism: a review. Sedimentology 15:281–346

Dutta PK, Suttner LJ (1986) Alluvial sandstone composition and paleoclimate, II. Authigenic Mineralogy. J Sediment Res 56:346–358

Fesharaki O, García-Romero E, Cuevas-Gonzalez J, López-Martínez N (2007) Clay mineral genesis and chemical evolution in the Miocene sediments of Somosaguas, Madrid Basin, Spain. Clay Miner 42:187–201

He B, Xu Y, Chuang S, Long X, Wang Y (2003) Sedimentary evidence for a rapid, kilometer-scale crustal doming prior to the eruption of the Emeishan flood basalts. Earth Planet Sci Lett 213:391–405

He B, Xu YG, ZhongYT GJP (2010) The Guadalupian-Lopingian boundary mudstones at Chaotian (SW China) are clastic rocks rather than acidic tuffs: implication for a temporal coincidence between the end-Guadalupian mass extinction and the Emeishan volcanism. Lithos 119:10–19

He H, Li T, Tao Q, Chen T, Zhang D, Zhu J, Yuan P, Zhu R (2014) Aluminum ion occupancy in the structure of synthetic saponites: effect on crystallinity. Am Mineral 99(1):109–116

He H, Ji S, Tao Q, Zhu J, Chen T, Liang X, Li Z, Dong H (2017) Transformation of halloysite and kaolinite into beidellite under hydrothermal condition. Am Mineral 102:997–1005

Hou Y, Zhong Y, Xu Y, He B (2017) The provenance of late Permian karstic bauxite deposits in SW China, constrained by the geochemistry of interbedded clastic rocks, and U-Pb-Hf-O isotopes of detrital zircons. Lithos 278–281:240–254

Huang J, He H, Tan W, Liang X, Ma L, Wang Y, Qin X, Zhu J (2021) Groundwater controls REE mineralisation in the regolith of South China. Chem Geol 577:120295

Huang Z, Jin Z, Xiang X, Gu J, Wu G, Chen X, Su Z, Zhao Y, Ye L, Zhou L (2014) Metallogenic theory and prediction of Wuchuan–zhengan–daozhen bauxite deposits in northern Guizhou, China. Beijing, Science Press. pp 1–245 (in Chinese).

International Energy Agency (2022) World Energy Outlook 2022, https://www.Iea.org/t&c/

Ji S, Zhu J, He H, Tao Q, Zhu R, Ma L, Chen M, Li S, Zhou J (2018) Conversion of serpentine to smectite under hydrothermal condition: implication for solid-state transformation. Am Mineral 103:241–251

Kesler SE, Gruber PW, Medina PA, Keoleian GA, Everson MA, Wallington TJ (2012) Global lithium resources: relative importance of pegmatite, brine and other deposits. Ore Geol Rev 48:55–69

Lanson B, Beaufort D, Berger G, Baradat J, Lacharpagen JC (1996) Illitization of diagenetic kaolinite-to-dickite conversion series: late-stage diagenesis of the Lower Permian Potliegend sandstone reservoir, offshore of the Netherlands. J Sediment Res 66:501–518

Lanson B, Beaufort D, Berger G, Bauer A, Cassagnabère A, Meunier A (2002) Authigenic kaolin and illitic minerals during burial diagenesis of sandstones: a review. Clay Miner 37:1–22

Li MYH, Zhou MF, Williams-Jones AE (2020) Controls on the dynamics of rare earth elements during subtropical hillslope processes and formation of regolith hosted deposits. Econ Geol 115:1097–1118

Ling K, Wen H, Zhang Q, Luo C, Gu H, Du S, Yu W (2021) Superenrichment of lithium and niobium in the Upper Permian Heshan Formation in Pingguo, Guangxi, China. Sci China Earth Sci 64:753–772

Liu X, Wang Q, Zhang Q, Yang S, Liang Y, Zhang Y, Li Y, Guan T (2017) Genesis of the Permian karstic Pingguo bauxite deposit, western Guangxi, China. Miner Deposita 52(7):1031–1048

Lu Z, Hu R, Han T, Wen H, Mo B, Algeo TJ (2021) Control of V accumulation in organic-rich shales by clay-organic nanocomposites. Chem Geol 567:120100

Ma C, Eggleton RA (1999) Cation exchange capacity of kaolinite. Clay Clay Miner 47:174–180

Muffler LJP, White DE (1969) Active metamorphism of Upper Cenozoic sediments in the Salton Sea geothermal field and the Salton Trough, southeastern California. Geol Soc Am Bull 80(2):157–182

Nadeau PH, Wilson MJ, McHardy WJ, Tait JM (1985) The conversion of smectite to illite during diagenesis: evidence from some illitic clays from bentonites and sandstones. Miner Mag 49:393–400

Robinson D, Schmidt ST, Santana de Zamora A (2002) Reaction pathways and reaction progress for the smectite-to-chlorite transformation: evidence from hydrothermally altered metabasites. J Metamorph Geol 20:167–174

Shellnutt JG (2014) The Emeishan large igneous province: a synthesis. Geosci Front 5:369–394

Shen L, Song Y, Peng Z, Guo K (1986) Discovery and preliminary study of Li-chlorite in claystone from a certain location of Henan province. Acta Miner Sin 6:86–91 (in Chinese with English abstract)

Smith JT, Ehrenberg SN (1989) Correlation of carbon dioxide abundance with temperature in clastic hydrocarbon reservoirs: relationship to inorganic chemical equilibrium. Mar Petrol Geol 6(2):129–135

Sommer F (1978) Diagenesis of Jurassic sandstones in the Viking Graben. J Geol Soc 135:63–67

Song Y, Shen L, Zhang N, Peng Z, Guo K (1987) A preliminary study on clay minerals and REE and Li in clay ore (rocks) in Henan Province. Sci China Ser B 59:324–326

Sun Y, Lai X, Wignall PB, Widdowson M, Ali JR, Jiang H, Wang W, Yan C, Bond DPG, Vedrine S (2010) Dating the onset and nature of the middle Permian Emeishan large igneous province eruptions in SW China using conodont biostratigraphy and its bearing on mantle plume uplift models. Lithos 119:20–33

Tao Q, Xing C, Lee S, Yang L, Zeng Q, Li S, Zhang T, Lv G, He H, Komarneni S (2022) Local structure determination of Zn-smectite. Am Mineral. https://doi.org/10.2138/am-2022-8591

Tinto R (2022) Update to ore reserves and mineral resources at Jadar. Rio Tinto Ltd

Tosca NJ, Johnston DT, Mushegian AM, Rothman DR, Roger E, Summons RE, Knoll AH (2010) Clay mineralogy, organic carbon burial, and redox evolution in Proterozoic oceans. Geochim Cosmochim Acta 74:1579–1592

USGS (2023) Mineral commodity summaries 2023. U.S. Geological Survey, https://www.usgs.gov/publications/mineral-commodity-summaries-2023.

Verley CG, Geo P (2014) Updated and reclassified lithium resources. Sonora Lithium Project

Wang Q, Liu X, Yan C, Cai S, Li Z, Wang Y, Zhao J, Li G (2012) Mineralogical and geochemical studies of boron-rich bauxite ore deposits in the Songqi region, SW Henan, China. Ore Geol Rev 48:258–270

Wang D, Li P, Qu W, Yin L, Zhao Z, Lei Z, Wen S (2013) Discovery and preliminary study of the high tungsten and lithium contents in the Dazhuyuan bauxite deposit, Guizhou, China. Sci China Earth Sci 56:145–152

Wen H, Luo C, Du S, Yu W, Gu H, Ling K, Cu Y, Li Y, Yang J (2020) Carbonate-hosted clay-type lithium deposit and its prospecting significance. Chin Sci Bull 65:53–59 (in Chinese with English abstract)

Worden RH, Griffiths J, Wooldridge LJ, Utley JEP, Lawan AY, Muhammed DD, Simon N, Armitage PJ (2020) Chlorite in Sandstones Earth-Sci Rev 204:103105

Yang S, Wang Q, Deng J, Wang Y, Kang W, Liu X, Li Z (2019) Genesis of karst bauxite-bearing sequences in Baofeng, Henan (China), and the distribution of critical metals. Ore Geol Rev 115:103161

Yang YX, Zhang NX (1994) Clay minerals of China. Geological Publishing House, Beijing, pp 1–297 (in Chinese)

Yu W, Algeo TJ, Yan J, Yang J, Du Y, Huang X, Weng S (2019) Climatic and hydrologic controls on upper Paleozoic bauxite deposits in South China. Earth-Sci Rev 189:159–176

Zhang J, Wang Q, Liu X, Zhou G, Xu H, Zhu Y (2022) Provenance and ore-forming process of Permian lithium-rich bauxite in central Yunnan, SW China. Ore Geol Rev 145:104862